Polymer 50 (2009) 4768–4774

Contents lists available at ScienceDirect

Polymer

journal homepage: www.elsevier.com/locate/polymer

PMMA–mesocellular foam silica nanocomposites prepared through batch emulsion polymerization and compression molding

Fa-Ai Zhang [a,b], Dong-Keun Lee [a], Thomas J. Pinnavaia [a,*]

[a] Department of Chemistry, Michigan State University, East Lansing, MI 48824, USA
[b] Laboratory of Nonferrous Materials and New Processing Technology, Ministry of Education, Department of Material and Chemical Engineering, Guilin University of Technology, Guilin, Guangxi 541004, PR China

ARTICLE INFO

Article history:
Received 15 May 2009
Received in revised form
3 August 2009
Accepted 4 August 2009
Available online 9 August 2009

Keywords:
Mesoporous silica
Nanocomposite
PMMA

ABSTRACT

PMMA–mesoporous silica nanocomposites were prepared for the first time through *in situ* batch emulsion polymerization of methyl methacrylate in the presence of large pore MSU-F silica with a mesocellular foam structure (24.8 nm average cavity size) and subsequent compression molding of the polymer–silica nanoparticle mixtures. For composites containing 5.0 wt % silica, the onset decomposition temperature and the temperature at 10% weight loss for the nanocomposite increased 41 °C and 50 °C, respectively, in comparison to pure PMMA. The glass transition temperature of the nanocomposite increased 9.3 °C, as determined by differential scanning calorimetry. In addition, the storage modulus determined by dynamic mechanical analysis increased 17% and 80% at 50 °C and 100 °C, respectively. Substantial improvements in tensile strength (+50%) and modulus (+72%), were achieve at 10 wt % nanoparticle loading. Composites made by compression molding of physical mixtures of PMMA and MSU-F silica powders provide less improvement in thermal stability, glass transition temperature and mechanical properties in comparison to the composites made through *in situ* batch emulsion polymerization. Unlike previously reported composites made from nanoclays, the silica composites reported here show improvements in both thermal stability and mechanical reinforcement.

1. Introduction

Polymer nanocomposites have received much attention recently due to the possibility of improving the mechanical, thermal, optical and barrier properties in comparison to the pure polymer. A number of review papers have described polymer-layered silicate [1–4], polymer–carbon nanotube (CNT) [2,5], polymer–silica [6,7] and other nanocomposites [8,9]. Poly(methyl methacrylate) (PMMA) has been widely utilized as a model thermoplastic polymer matrix because it can be easily polymerized by several different polymerization techniques [10–12]. PMMA exhibits a high modulus and good thermal stability, but the polymer in nanocomposite form might provide added benefits in mechanical and thermal properties.

Surfactant-templated mesoporous forms of silica are of materials interest due in part to their large surface areas, uniform framework structures and readily controlled pore diameters [13]. These porous solids may be used as catalysts [14,15], absorbents and chromatographic materials [16,17], chemical sensors [18], optical/electric devices [19], and reinforcing agents in polymer nanocomposites [20]. For nanocomposite applications, the nanoscale porous silica acts as the host and the polymer acts as the pore guest. Due to favorable guest–host interactions these nanocomposites can possess substantially improved mechanical and thermal properties. Various types of monomers, including ethylene [21,22], propylene [23], aniline [24,25], pyrrole [26,27], vinyl acetate [28], styrene [29], among others, have been polymerized within the channels of hexagonal MCM-41, cubic MCM-48 and hexagonal SBA-15 silicas and the properties of the resulting nanocomposites have been examined.

We previously showed that rubbery epoxy mesocomposites formed from framework MSU-J silica with a wormhole framework structure and large pores (5.3 nm), exhibited an enhanced tensile modulus, strength, toughness, and extension-at-break, in comparison to the pure epoxy polymer [30,31]. A new kind of mesoporous silica with exceptionally large pore size (25 nm) and a mesocellular foam structure (denoted MSU-F) [32] also is a good reinforcement agent for rubber epoxy [33] due in part to its large surface area, pore size and pore volume. Although methyl methacrylate (MMA) has been polymerized within the pores of several

* Corresponding author. Tel.: +1 517 432 1222; fax: +1 517 432 1225.
E-mail address: pinnavaia@chemistry.msu.edu (T.J. Pinnavaia).

0032-3861/$ – see front matter © 2009 Elsevier Ltd. All rights reserved.
doi:10.1016/j.polymer.2009.08.007

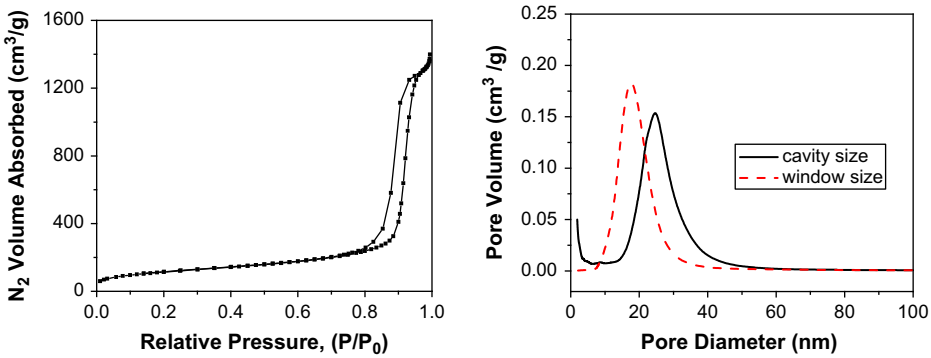

Fig. 1. N_2 absorption and desorption isotherms (left) and window and cavity size distributions (right) for mesoporous MSU-F silica nanoparticles after calcination at 600 °C.

forms of mesoporous silica [34–37], mesocellular MSU-F silica has not yet examined as a reinforcing agent for PMMA. Mollers et al. [36] have synthesized host–guest composites of PMMA within the pores of zeolites ZSM-5 and NaY, and the silica mesophases MCM-41 and MCM-48. The confined polymer did not exhibit a glass transition temperature, indicating strong interaction of the polymer with the pore surfaces. Run et al. [13] prepared PMMA-cubic MCM-48 silica composites by *in situ* polymerization and found that the thermal stability, glass transition temperature, tensile strength, and Young's modulus of the resulting composites increased with increasing silica loading.

Very few studies are reported for the preparation of polymer–mesoporous silica nanocomposites via emulsion polymerization in water media. Wei and Zhang [38] provided a recent example of nanocomposite formation through ethylene emulsion polymerization in the presence of vinyl-functionalized mesoporous silica nanoparticles. Emulsion polymerization also is an effective and environmental-friendly method for forming PMMA with high molecular weight, but to our knowledge, this approach is not reported for the preparation of PMMA–mesoporous silica nanocomposites. In this paper we report for the first time PMMA–mesoporous silica nanocomposites made by compression molding of large pore MSU-F mesocellular silica and PMMA nanoparticle via batch emulsion polymerization and subsequent compression molding.

2. Experimental

2.1. Materials

Methyl methacrylate (MMA, 99%), reagent grade ammonium persulfate (APS, 98%), sodium dodecyl sulfate (SDS), and nonionic surfactant TERGITOL NP-9 were purchased from Sigma–Aldrich Co. J.T. Baker chemical Co. provided analytical reagent grade aluminum sulfate. Sodium bicarbonate (reagent grade) was from Spectrum Quality Products Inc. MMA was distilled under reduced pressure before use. The remaining reagents were used as received. Deionized water was used in all experiments. Mesocellular foam silicate MSU-F was prepared from sodium silicate, Pluronic P123 surfactant and mesitylene as the cosurfactant according to literature methods [32]. The as-made MSU-F was calcined at 600 °C for 6 h to remove the surfactant from the mesopores.

2.2. Preparation of PMMA–MSU-F nanocomposites by emulsion polymerization and compression molding

Emulsion polymerization reactions were carried out in a 250-ml glass reactor equipped with a reflux condenser, stainless-steel stirrer, and thermometer. The polymer content of the emulsion was ~40% by weight. For the *in situ* batch emulsion polymerization procedure (denoted Method A), water (90 g), MMA monomer (60 g), NP-9 (1.2 g), SDS (1.2 g), sodium dicarbonate (0.2 g), APS (0.18 g) and MSU-F (3.0 g or 6.0 g) were charged in the reactor in the order stated. The reaction mixture was sonicated for 20 min to form the emulsion, followed by purging with nitrogen for 20 min to remove oxygen, and then heated to 75 °C to initiate polymerization. After a reaction time of 3 h, the emulsion was demulsified by the addition of a 10% aqueous solution of $Al_2(SO_4)_3$. The solid products were filtered, washed thoroughly with water, and then dried at 60 °C in a vacuum oven for 24 h. The final PMMA–MSU-F silica nanocomposites were formed by compression molding at 250 °C and 170 MPa pressure.

We also investigated two alternative methods of combining the PMMA and MSU-F silica particles prior to forming the final nanocomposite by compression molding. In one case (method B), an aqueous suspension of MSU-F silica and a pure PMMA emulsion made by batch emulsion polymerization were sonicated for 30 min and then demulsified, filtered, washed, and dried prior to forming the nanocomposite by compression molding. In the other alternative procedure (Method C), dry powders of MSU-F and PMMA are blended for 30 min in a Venie 2 vortex blender (Fisher Science Co.) prior to compression molding.

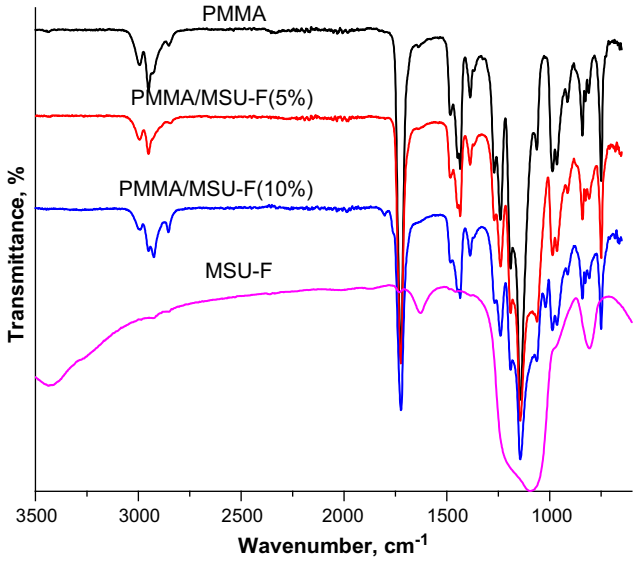

Fig. 2. FTIR spectra of MSU-F, PMMA and PMMA–MSU-F nanocomposites containing 5.0 and 10.0 wt % mesoporous MSU-F silica made by in situ batch polymerization and compression molding of the nanoparticle mixture at 250 °C (Method A). The spectra of the PMMA and PMMA–MSU-F film samples were measured by ATR, whereas the spectrum of the MSU-F was obtained in transmission mode on a KBr pellet sample.

2.3. Physical measurements

N_2 adsorption–desorption isotherms were obtained at 77 K on a TRISTAR 3000 volumetric adsorption analyzer. MSU-F silica was oven-dried at 150 °C overnight. The cavity size and window size of the mesocellular foam structure were determined by applying the BJH model to the adsorption and desorption legs of the nitrogen isotherms, respectively. IR spectra of compression molded thin film samples were obtained on a PerkinElmer FT-IR spectrometer equipped with a universal ATR sampling accessory. A PerkinElmer Pyris analyzer operated in air over the temperature range 30–600 °C provided thermogravimetric analysis (TGA) curves in analog and differential mode. The heating rate was 10 °C/min. A TA Q100 differential scanning calorimeter (DSC) afforded the glass transition temperatures of the nanocomposites under a nitrogen atmosphere. The scan rate was 10 °C/min over the temperature range 30–180 °C. The *Tg* values for pure PMMA and PMMA–MSU-F nanocomposites were obtained from the second scan of the DSC curve. A TA dynamic mechanical analyzer DMA Q800 V20.8 Build 26 operated at a fixed frequency of 1 Hz was used to obtain values of Tan δ and the storage modulus (E'). The heating rate was set as 3 °C/min over the range 30–180 °C. The sheet samples were cut to 30 × 6.5 × 0.4 mm specimens for analysis. The same instrument was used to carry out stress–strain experiments in strain. The strain rate was set as 0.1% per min at 30 °C. The morphology of specimens was observed using a JEOL JEM-100CX II transmission electron microscope (TEM) operated at an accelerating voltage of 120 kV.

3. Results and discussion

3.1. MSU-F silica nanoparticles

Nitrogen absorption–desorption isotherms for MSU-F mesocellular foam silica, along with the BJH cavity and window size distributions obtained from these isotherms, are presented in Fig. 1. This silica mesophase affords a specific BET surface area of 393 m^2/g, average window and cavity sizes of 18.4 and 24.8 nm and a pore volume of 2.2 cm^3/g. In comparison to mesoporous MCM-41 and

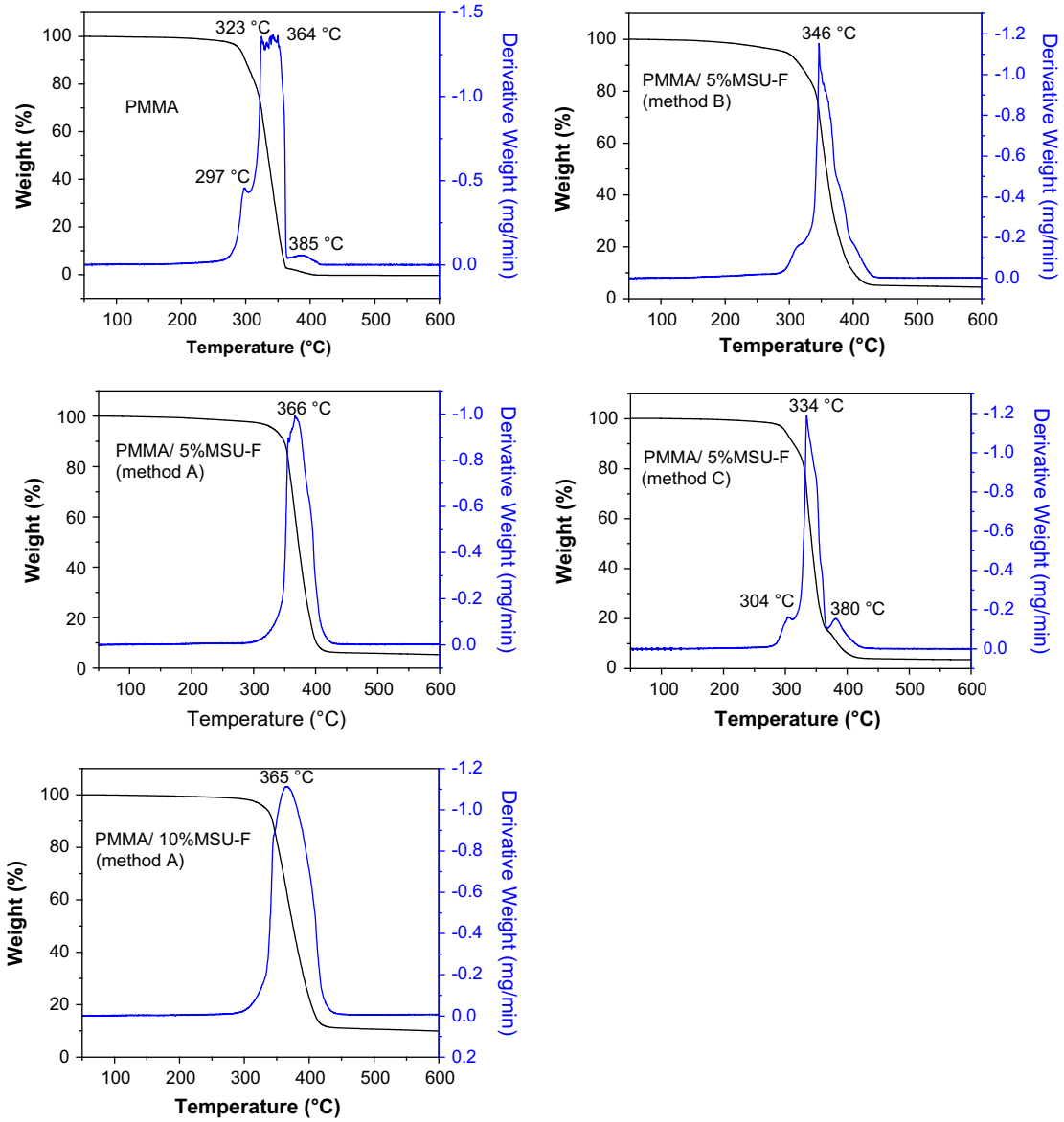

Fig. 3. Thermogravimetric analyses (TGA) and differential thermal gravimetric (DTG) curves for compression molded PMMA and the PMMA–MSU-F silica nanocomposites containing MSU-F silica. The polymer and silica nanoparticles were mixed by different methods prior to compression molding.

MCM-48 silicas with one-dimensional hexagonal and three-dimensional cubic pore system symmetries and small mesopores sizes (<3.5 nm), the MSU-F mesocellular foam structure exhibits an order of magnitude larger pore size. Thus, the larger and more open pore structure of MSU-F is more likely to facilitate polymer penetration of the intraparticle pores.

3.2. Fourier transform infrared spectra (FTIR) studies

Fig. 2 provides the FTIR spectra of PMMA, MSU-F silica and PMMA–MSU-F nanocomposites containing 5% and 10% (w/w) mesoporous MSU-F silica nanoparticles. The composites were by *in situ* emulsion polymerization in the presence of MSU-F silica, followed by compression molding at 250 °C to form the final composite (Method A). Pure PMMA exhibits a very strong C=O ester carbonyl stretching vibration at 1723 cm^{-1}. Two C–H stretching vibrations at 2950 and 2993 cm^{-1}, two strong bands at 1434 and 1448 cm^{-1} originating from the O–CH_3 bending vibrations, one very strong absorption at 1143 cm^{-1} associated with C–O stretching, and two adsorption bands at 1386 and 1482 cm^{-1} assigned to the C–H bending vibrations also are observed. As expected, PMMA–MSU-F nanocomposites show absorption peaks characteristic for the two phases. The carbonyl absorption remains at 1723 cm^{-1}, and the C–H stretching vibration (2950, 2993 cm^{-1}), O–CH_3 stretching bands (1435, 1448 cm^{-1}), C–O stretching band (1143 cm^{-1}) and C–H bending vibrations (1386 and 1482 cm^{-1}) are similar to those observed for pure PMMA. A strong absorption peak at 1061 cm^{-1} associated with Si–O stretch appears in the spectra for the MSU-F silica and PMMA–MSU-F nanocomposites. These results are in good agreement with previous papers describing PMMA nanocomposites [13,36].

Nanocomposites made by compression molding of PMMA and MSU-F nanoparticles mixed by dispersion in water (Method B) or by blending of dry powders (Method C) exhibit analogous IR spectra. Thus, the nature of the polymer–silica interface, as judged by infrared spectroscopy, is not greatly affected by the method used to achieve nanoparticle mixing prior to compression molding.

3.3. Thermogravimetric analysis (TGA)

The thermogravimetric curves provided in Fig. 3 for representative PMMA–MSU-F nanocomposites show that the thermal stabilities of the polymers are improved in the presence of MSU-F silica, regardless of the method used to mix the nanoparticle phases prior to compression molding. As shown in Table 1, the onset decomposition temperature (T_{onset}), the temperature at 10% (T_{10}) and 50% weight loss (T_{50}), the temperature at maximum weight loss rate (T_{max}) and the end decomposition temperature (T_{end}) are all increased. For example, T_{onset}, T_{10} and T_{end} for the nanocomposite containing 5% MSU-F silica made by Method A increase 41 °C, 50 °C and 36 °C, respectively, compared with pure PMMA. Additionally, the nanocomposites made by physical mixing Methods B and C exhibit higher thermal stability than pure PMMA, but the corresponding decomposition temperatures are lower in comparison to those obtained for the composites made by *in situ* polymerization. This indicates that *in situ* polymerization Method A provides a better dispersion of MSU-F silica particles in the initially formed polymer (hence, a better compression molded composite) in comparison to Methods B and C, wherein the initial mixtures of PMMA and MSU-F particles are formed by mixing aqueous suspensions and dry powders of the two phases, respectively.

Fig. 3 provides the thermogravimetric analyses (TGA) and differential thermal gravimetric (DTG) curves for PMMA and the PMMA–MSU-F silica nanocomposites. In accord with previous observations [39], pure PMMA undergoes thermal decomposition

Table 1
Thermal decomposition temperatures for PMMA and PMMA–MSU-F nanocomposites.

MSU-F silica content (%)	Nanoparticle mixing method[a]	$T_{on\text{-}set}$ °C	T_{10} °C	T_{50} °C	T_{max} °C	T_{end} °C
0	–	307	299	333	297,323,364	360
5	A	348	349	371	366	396
10	A	336	342	374	365	406
5	B	330	316	356	346	388
5	C	317	313	342	304,334,380	367

[a] In Method A the PMMA particles were formed by *in situ* batch emulsion polymerization in the presence of MSU-F silica; in Methods B and C, the PMMA and silica nanoparticles were mixed in aqueous suspension and by dry powder blending prior to compression molding, respectively.

in two main stages. The lower temperature process involves unzipping of the chain starting at both the vinylidene end groups and the weaker head-to-head linkages. This unzipping process occurs at a higher temperature in air than in nitrogen due to the formation of more stable peroxide radical intermediates under aerobic conditions [40]. Because the vinylidene end groups and head-to-head linkages represent 28% and 36% of the total fraction of polymer molecules, respectively, the unzipping process is an important degradation pathway [40]. The second stage decomposition involves random scission of the polymer chains.

Under aerobic conditions, pure PMMA clearly displays these two reaction stages, whereas the PMMA–MSU-F nanocomposites display mainly the second decomposition stage. It is unlikely that the presence of silica substantially reduces the relative abundance of vinylidene end groups and head-to-head linkages because the IR spectrum of the polymer is qualitatively identical for both the pure polymer and the nanocomposites (c.f., Fig. 2). Previous studies of PMMA composites made from montmorillonite clay and synthetic zeolites suggested the scavenging of radical species by silicate phase, thus contributing to an improvement in thermal stability [41,42]. The MSU-F silica used in the present work may play an analogous radical scavenging role toward improving the thermal stability of the polymer matrix. On the other hand, the improved thermal stability may be a manifestation of the intrinsic stiffening of the polymer chains in the nanocomposite. As indicated by the substantial increases in T_g values (see below), interfacial

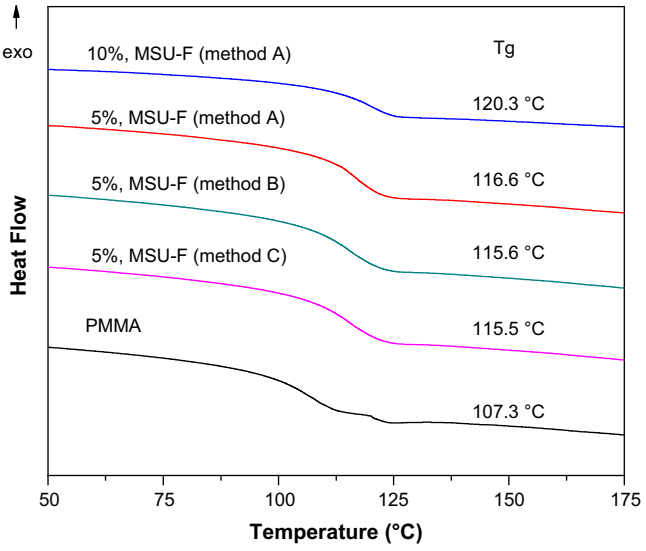

Fig. 4. DSC curves and T_g values for PMMA and PMMA–MSU-F nanocomposites prepared by different nanoparticle mixing method prior to compression molding.

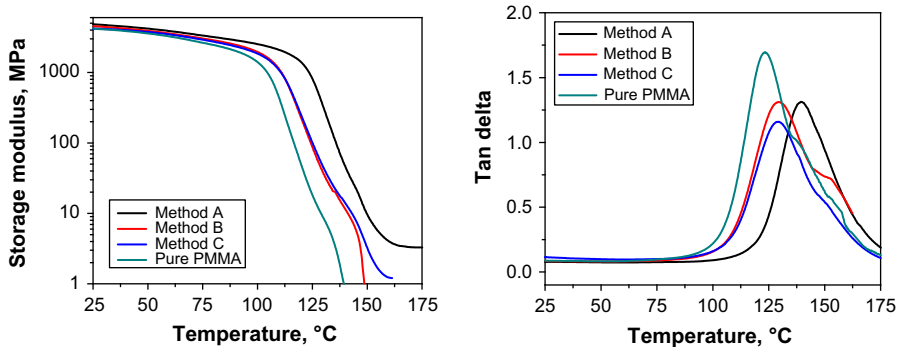

Fig. 5. DMA curves and tan δ plots for PMMA and PMMA – MSU-F nanocomposites prepared by *in situ* emulsion polymerization Method A, B and C at silica loadings of 5.0 wt %.

interactions between the silica and polymer leads to a polymer interphase that extends between silica nanoparticles and results a restriction of segmental motions along the polymer chain. Such restricted motions also may be manifested as a reduction in intrinsic thermal reactivity.

The improvements in thermal stability for the composites made by Method A are superior to those reported for PMMA–layered double hydroxide (LDH) and PMMA–organoclay composites. For instance, the respective T_{10} values for the latter composites are 19 and 35 °C higher than the pure polymer, whereas an improvement of 50 °C is realized for the PMMA–MSU-F composite made by Method A [43]. It is noteworthy, however, that PMMA–carbon nanotube composites provide a 60 °C improvement in T_{10} [43].

3.4. Differential scanning calorimetry (DSC)

Fig. 4 illustrates the transition behavior of pure PMMA and the PMMA–MSU-F nanocomposites as measured by DSC. T_g for the pure PMMA is 107.3 °C, whereas all the PMMA–MSU-F nanocomposites exhibit substantially higher T_g values. For the PMMA–MSU-F nanocomposites made by *in situ* emulsion polymerization Method A, the T_g increases to 116.6 and 120.3 °C at loadings of 5% and 10% MSU-F, i.e., increases of 9.3 and 13 °C, respectively. The 5 wt% composites made by nanoparticle mixing Methods B and C exhibit a somewhat lower T_g in comparison to the composite made by Method A, but the T_g values remain substantially higher than observed for the pure polymer. Nevertheless, substantial interfacial interactions between the polymer and silica also are achieved through compression molding of powdered polymer and silica mixtures. The superior stability of the composite made by *in situ* batch polymerization is attributed to the more intimate initial mixing of the nanoparticles in comparison to the physical mixing of PMMA and MSU-F powders (see TEM results below).

As shown by several earlier studies, the confinement of PMMA in the gallery region of layered silicate clays [43], in the micropores of zeolites [36] and the mesopores surfactant-templated silica [13,36] results in the loss of a second-order phase transition. Although not supported by a low frequency shift in carbonyl stretching frequency, the physical interaction of the PMMA filaments with the wall of host silicate is sufficiently strong to form an interphase region that extends tens of nanometers from the silicate surface and restricts the segmental motion of the chains. The reduction in the pore-wall contrast in the TEM images described below indicates that PMMA penetrates the 22 nm mesopores of the MSU-F silica under compression molding conditions (250 °C, 170 MPa). Consequently, we do not expect a T_g for the polymer fraction confined in framework mesopores. This means that the observed increase in T_g almost certainly is associated with the PMMA external to the pores of the silica and reflects the reduction in segmental motions for the polymer fraction that occupies space between particles (~90% of the total polymer at 5.0 wt % loading).

3.5. Dynamic mechanical analysis (DMA) and tensile properties

The storage modulus of PMMA–MSU-F nanocomposites containing different loadings of MSU-F silica were determined over the temperature range 30–180 °C. For a PMMA–MSU-F nanocomposite with a 5 wt % silica loading, the storage modulus increases 17% and 80% at 50 °C and 100 °C, respectively, in comparison to the pristine polymer. The maximum in the tan δ plots shifts from 123.7 °C for pure PMMA to 139.4 °C at 5% MSU-F loading. Thus, in addition to improving the thermal stability of the PMMA matrix and restricting the segmental motion of the bulk polymer chains in the matrix, MSU-F silica functions also as a reinforcing agent. As shown in Fig. 5, a 5 wt% PMMA–MSU-F nanocomposites prepared by nanoparticle mixing Methods B and C exhibit a lower storage modulus in comparison to Method A, though still higher than pure PMMA. In addition, the T_g values as determined from the maxima in the tan δ plots (128.7 and 129.2 °C, respectively) are lower than the composite made by Method A, but still higher than the T_g for pure PMMA.

Fig. 6 displays stress–strain curves for the PMMA and PMMA–MSU-F nanocomposites. These curves show that Young's modulus increases substantially upon incorporation of MSU-F silica in the

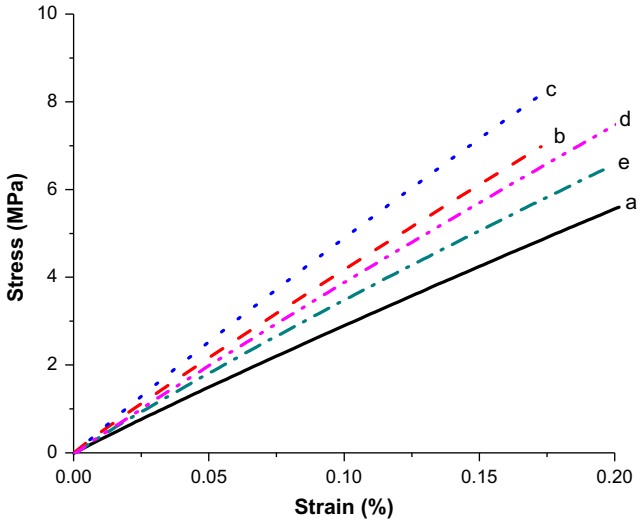

Fig. 6. Stress–strain curves for: (a) pure PMMA polymer; (b) and (c) PMMA–MSU-F nanocomposites made by Method A containing 5% and 10% MSU-F silica, respectively; and (d) and (e) composites containing 5 wt % MSU-F silica made by Methods B and C, respectively.

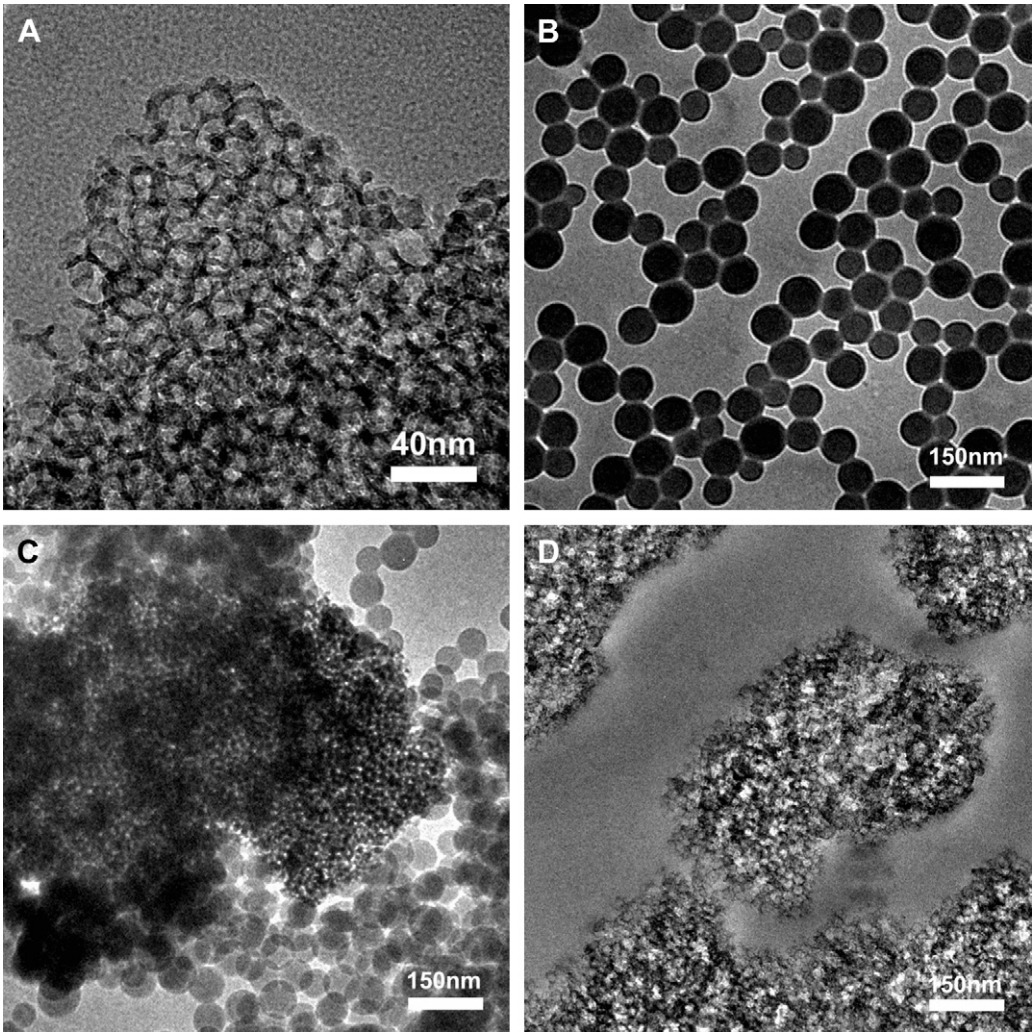

Fig. 7. TEM images for (A) a MSU-F silica nanoparticle, (B) pure PMMA nanoparticle made by emulsion polymerization, (C) the PMMA–MSU-F mixture made by *in situ* emulsion polymerization Method A and (D) a thin sectioned specimen of the 5.0 wt% nanocomposite formed by compression molding a MSU-F and PMMN nanoparticle mixture formed by *in situ* batch polymerization Method A.

PMMA matrix. The strength and modulus increase by 50% and 72%, respectively, at a 10% loading. In addition, the nanocomposite made by *in situ* emulsion polymerization Method A exhibits a higher modulus in comparison to composites made by Methods B and C. The results further show that MSU-F silica is a very effective reinforcement agent for PMMA especially when nanoparticle mixing is achieved through *in situ* emulsion polymerization prior to compression molding.

3.6. Transmission electron microscopy (TEM) images

The TEM image in Fig. 7 (a) shows the mesopore morphology of typical MSU-F silica. The window and cell sizes of the mesocellular foam structure are in agreement with the values obtained from the nitrogen adsorption and desorption isotherm in Fig. 1. The image in Fig. 7 (b) shows the regularity of the spherical PMMA nanoparticles ($\sim$100) nm made by emulsion polymerization. Fig. 7 (c) shows that the *in situ* batch polymerization of PMMA in the presence of MSU-F silica (Method A) results in an intimate nanoparticle mixture in which the PMMA particles cling to the silica particles. Analogous electrostatic interactions are absent in physical mixtures of particles made by Methods B and C, most likely because these latter methods do not expose the particles to the pH conditions encountered in Method A. The lack of such interparticle interactions reduces the level of silica dispersion in the PMMA polymer and in the corresponding compression molded composites, thus accounting for the reduction in performance properties in comparison to specimens made by Method A.

The high contrast between the silica walls and the open framework pores of the silica mesostructure indicates that the pores are open and occupied by PMMA during the polymerization process. However, for the compression molded specimen made by Method A (Fig. 7 (d)), the contrast between the silica walls and pores is diminished, which is indicative of the penetration of PMMA into the framework under melt processing conditions. As noted above, the intercalated fraction of polymer does not contribute to the observed T_g. Only the polymer fraction external to the pores exhibits a second order transition temperature.

4. Conclusions

Mesoporous MSU-F silica with a mesocellular foam structure and window and pore sizes of 18.4 and 24.8 nm is very effective in forming PMMA nanocomposites by compression molding of

nanoparticle mixtures prepared by *in situ* batch free radical emulsion polymerization. The resulting nanocomposites exhibit a substantially improved thermal stability, an elevated glass transition temperature, and an enhanced storage modulus, Young's modulus and tensile strength in comparison to the pure polymer. Qualitatively analogous benefits are reported for PMMA composites made from small pore (3.0 nm) MCM-48 silica by bulk polymerization methods. However, the bulk polymerization approach requires mesopore pore out-gassing prior to polymerization and faces inherent problem of non-uniform particle dispersion in the polymer matrix.

The improvements in thermal and mechanical properties achieved for PMMA in the present work exceed those reported for PMMA–organoclay nanocomposites. The dispersion of clay nanoparticles in PMMA normally requires organic modification of the clay surface [42,43] or the introduction of cationic sites on the PMMA chains to achieve compatibility [44]. Neither modification is needed for particle dispersion using the methodology described in the present work. Purely inorganic sodium montmorillonite clay is known to provide some improvement in thermal stability for composites made by emulsion polymerization and subsequent melt processing [44]. However, the clay provides only marginal increases in tensile strength (15%) and Young's modulus (19%) at 10 wt % loading. The benefits in tensile properties most likely are limited by the plasticizing effect of the organoclay surface modifiers. The PMMA–MSU-F silica composites described in the present work are free of organic surface modifiers and afford improvements of 50% and 72% in strength and modulus, respectively, at 10% loading.

Acknowledgements

We acknowledge the support of the State Scholarship Fund from the China Scholarship Council.

References

[1] Morgan AB. Polym Adv Technol 2006;17(4):206–17.
[2] Hussain F, Hojjati M, Okamoto M, Gorga RE. J Compos Mater 2006;40(17):1511–75.
[3] Liu J, Boo WJ, Clearfield A, Sue HJ. Mater Manuf Processes 2006;21(2):143–51.
[4] Okada A, Usuki A. Macromol Mater Eng 2006;291(12):1449–76.
[5] Ahir SV, Huang YY, Terentjev EM. Polymer 2008;49(18):3841–54.
[6] Zeng QH, Yu AB, Lu GQ. Prog Polym Sci 2008;33(2):191–269.
[7] Zou H, Wu SS, Shen J. Chem Rev 2008;108(9):3893–957.
[8] Balazs AC, Emrick T, Russell TP. Science 2006;314(5802):1107–10.
[9] Paul DR, Robeson LM. Polymer 2008;49(15):3187–204.
[10] Kong QH, Hu Y, Yang L, Fan WC, Chen ZY. Polym Compos 2006;27(1):49–54.
[11] Qu XW, Guan TJ, Liu GD, She QY, Zhang LC. J Appl Polym Sci 2005;97(1):348–57.
[12] Xie TX, Yang GS, Fang XP, Ou YC. J Appl Polym Sci 2003;89(8):2256–60.
[13] Run MT, Wu SZ, Zhang DY, Wu G. Mater Chem Phys 2007;105(2–3):341–7.
[14] Haller GL. J Catal 2003;216(1–2):12–22.
[15] Lin HP, Cheng YR, Lin CR, Li FY, Chen CL, Wong ST, et al. J Chin Chem Soc 1999;46(3):495–507.
[16] Choi M, Kleitz F, Liu DN, Lee HY, Ahn WS, Ryoo RJ. Am Chem Soc 2005;127(6):1924–32.
[17] Peng XS, Jin J, Ichinose I. Adv Funct Mater 2007;17(11):1849–55.
[18] Geng WC, Li XT, Li N, Zhang T, Wang W, Qiu SL. J Appl Polym Sci 2006;102(4):3301–5.
[19] O'Neil A, Watkins JJ. MRS Bull 2005;30(12):967–75.
[20] Fujiwara M, Kojima K, Tanaka Y, Nomura R. J Mater Chem 2004;14(7):1195–202.
[21] Aguado J, Callej G, Carrero A, Moreno J. Chem Eng J 2008;137(2):443–52.
[22] Kageyama K, Tamazawa J, Aida T. Science 1999;285(5436):2113–5.
[23] Dong XC, Wang L, Wang JJ, Zhou JF, Sun TX. J Phys Chem B 2006;110(18):9100–4.
[24] Wu CG, Bein T. Science 1994;264(5166):1757–9.
[25] Sasidharan M, Mal NK, Bhaumik A. J Mater Chem 2007;17(3):278–83.
[26] Jang JS, Lim B, Lee J, Hyeon T. Chem Commun 2001;(01)::83–4.
[27] Nakayama M, Yano J, Nakaoka K, Ogura K. Synth Met 2002;128(1):57–62.
[28] He J, Shen YB, Yang J, Evans DG, Duan X. Chem Mater 2003;15(20):3894–902.
[29] Uemura T, Horike S, Kitagawa K, Mizuno M, Endo K, Bracco S, et al. J Am Chem Soc 2008;130(21):6781–8.
[30] Park I, Peng HG, Gidley DW, Xue SQ, Pinnavaia TJ. Chem Mater 2006;18(3):650–6.
[31] Jiao J, Sun X, Pinnavaia TJ. Adv Funct Mater 2008;18(7):1067–74.
[32] Kim SS, Pauly TR, Pinnavaia TJ. Chem Commun 2000;17:1661–2.
[33] Park I, Pinnavaia TJ. Adv Funct Mater 2007;17(15):2835–41.
[34] Audouin F, Blas H, Pasetto P, Beaunier P, Boissiere C, Sanchez C, et al. Macromol Rapid Commun 2008;29(11):914–21.
[35] Moller K, Bein T, Fischer RX. Chem Mater 1999;11(3):665–73.
[36] Moller K, Bein T, Fischer RX. Chem Mater 1998;10(7):1841–52.
[37] Valsesia P, Beretta M, Bracco S, Comotti A, Sozzani P. J Mater Chem 2008;18(45):5511–7.
[38] Wei L, Zhang Y. J Polym Sci Part A Polym Chem 2009;47:1393–402.
[39] Hirata T, Kashiwagi T, Brown JE. Macromolecules 1985;18(7):1410–8.
[40] Kashiwagi T, Inaba A, Brown JE, Hatada K, Kitayama T, Masuda E. Macromolecules 1986;19(8):2160–8.
[41] Solomon DH, Swift JD. J Appl Polym Sci 1967;11(12):2567.
[42] Hwang KJ, Kim DS. J Appl Polym Sci 2008;110(5):2957–60.
[43] Effenberger F, Schweizer M, Mohamed WS. J Appl Polym Sci 2009;112(3):1572–8.
[44] Lee DC, Jang LW. J Appl Polym Sci 1996;61(7):1117–22.